TECHNICAL MEMORANDUMS

NATIONAL ADVISORY COMMITTEE FOR AERONAUTICS

No. 777

TESTS OF SPHERES WITH REFERENCE TO REYNOLDS NUMBER, TURBULENCE, AND SURFACE ROUGHNESS

By S. Hoerner

Luftfahrtforschung
Vol. XII, No. 1, March 28, 1935
Verlag von R. Oldenbourg, München und Berlin

Washington
October 1935

NATIONAL ADVISORY COMMITTEE FOR AERONAUTICS

TECHNICAL MEMORANDUM NO. 777

TESTS OF SPHERES WITH REFERENCE TO REYNOLDS NUMBER, TURBULENCE, AND SURFACE ROUGHNESS*

By S. Hoerner

SUMMARY

The behavior of the Reynolds Number of the sphere is explained (in known manner) with the aid of the boundary-layer theory.

Rear spindles may falsify, under certain conditions, the supercritical sphere drag (fig. 3), while suspension wires in the space behind the sphere leave no traceable influence.

Depending upon its diameter, a centrally located rear spindle lowers the supercritical resistance substantially, because it induces the flow to adhere. To arrive at a diameter which remains practically ineffective from the point of supercritical resistance, is difficult, because in order to assure a safe and non-oscillating support, the spindle must be of a certain minimum cross section.

The subcritical resistance and the start of the transition is not affected by a rear support, thus making spindle diameters up to 1/4 sphere diameter permissible. Turbulence measurements with the aid of the sphere as indicator are not affected by rear support methods; spindle diameters over 0.2 D are permissible.

Contrariwise, the degree of surface roughness has a decisive effect upon sphere turbulence measurements, making accurately designed, mirror-polished (metal) spheres a necessity. The effect of surface texture was quantitatively determined from experiments.

---

*"Versuche mit Kugeln betreffend Kennzahl, Turbulenz und Oberflachenbeschaffenheit." Luftfahrtforschung, March 28, 1935, pp. 42-54.

The critical Reynolds Number of the sphere was arrived at by an unconventional method; that is, by determining the critical wind speed at which the static pressure at the back of the sphere is the same as that of the undisturbed flow. The method makes it possible to interpret the critical Reynolds Number with only one test station. Being extraordinarily simple, it lends itself extremely well to flight testing. Between p_{ru}'' and c_w there is a certain relationship.

The record of boundary-layer effective turbulence with a perfectly smooth 15-centimeter steel sphere in the wind tunnel at Braunschweiger, was a critical $R = 2.95 \times 10^5$, while the Reynolds Number of $R = 3.6 \times 10^5$, achieved with the same sphere in the 1.2-meter tunnel of the D.V.L. (status, 1935), surpasses any known measurement of this kind.

Measurements with different size spheres disclosed a decrease in effective turbulence with the speed for the investigated tunnels (fig. 9). The contraction in channel section lowered the turbulence perceptibly.

In consideration of the turbulence grid the turbulence (vortex street) set up by individual wires, was explored in detail through sphere tests.

Proof was adduced that the boundary layer of the sphere can be acoustically disturbed (through a strong whistling tune). The drop for the 15-centimeter sphere was from $R_k = 3.50$ to 2.40×10^5.

The critical Reynolds Numbers of various spheres were explored in free air in flight and towing tests. In still air and in wind free of obstacles, the same critical Reynolds Numbers were observed: $R_k = 3.95$ to 4.05×10^5. The boundary effective turbulence of the free atmosphere is very low ($R_k = 3.90$ in squally weather). Spheres protected against external vibrations will probably reveal still higher figures.

The surface roughness has a particularly great effect on the supercritical resistance. The knowledge regarding surface is applied to the sphere tests in the tunnel.

The deductions from the sphere tests relative to bodies of low drag are as follows:

The degree of surface roughness is most important of all. Any irregularity in form (steps) or roughness is at the expense of boundary-layer energy; the form drag increases disproportionately. On airplane bodies, for example, offsets, joints, and fittings should be treated much more carefully than at present. The effects of expensive design, outer finish, etc., are neutralized in many cases by seemingly secondary defects. From the practical point of view, the Reynolds Number (above the critical range) is of totally subordinate importance compared to the degree of surface roughness.

1. INTRODUCTION

a) Generalities

In conformity with the laws of the frictionless potential flow, the flow at the back of a body in inviscid fluid is reunited in the same measure as it is separated at the front. The positive (dynamic) pressure at back and front are the same and the resistance is zero.

In viscous fluid a frictional or boundary layer, i.e., a layer of diminished velocity, forms along the body surface. The purely frictional resistance matches the loss of momentum of the boundary layer due to the friction.

On interference bodies the boundary layer has a much more significant effect, namely, it initiates, according to Prandtl's boundary-layer theory (references 4 and 5), the breakdown of the flow at the back of the body.

Negative pressure prevails at the sides of the body, the amount of which is allied with the flow velocity according to Bernoulli's law; so the negative pressure varies, depending on the body form. On a vertically exposed thin disk, for example (fig. 1a), it is very high (infinitely high, theoretically), whereas flow velocity and negative pressure are low on streamlined bodies.

In frictionless fluid, the surface pressure would increase toward the rear stagnation point from negative, relative to undisturbed flow, to a positive maximum (dynamic pressure). But, in reality, the motion energy of the boundary layer, slowed up through friction, is not quite sufficient to overcome this pressure rise altogether.

Rather, the back pressure lowers the velocity of the boundary layer still further; indeed, the air particles moving in the layer come at rest under certain conditions. Piling up, they cause the flow to separate at the rear of the body; forces diverting the flow filaments into the created air space are nonexistent. The arrested boundary-layer particles intermingle with the outer flow and are entrained in separate vortex balls.

The subsequent rise of pressure at the back of the body is diminished in proportion to the velocity decrease of the boundary layer and the breakdown of the flow. The air space approximately assumes the pressure of the bordering flow filaments. (Compare with sphere in fig. 2.) The ensuing air resistance is the so-called pressure or form resistance. Consequently, the boundary layer stipulates not only the pure frictional resistance; it rather constitutes the "relay" to the often incomparably greater form resistance on real bodies.

The body form of minimum air resistance is the spindle (fig. 1d). Its coefficient of resistance (referred to maximum section) is $c_w \approx 0.05$, or about 4 percent of the disk of figure 1a. The pressure rise at the back of the spindle is voided by the consistent and progressive taper, as prescribed for diffusers; for example, when breakdown of flow is to be counteracted. The boundary layer draws the motion energy necessary for overcoming the pressure rise, little by little, from undisturbed flow through intermingling.

b) Boundary Layer Behavior on the Sphere

Figure 2 illustrates the pressure distribution over the sphere according to potential theory. The negative pressure at the equator is $-1.25\ q$. The boundary layer does not, in fact, share the reincrease of pressure to $+1\ q$ in the rear stagnation point; on the contrary, the flow separates at first entirely from the back of the sphere (fig. 1b).

Eiffel's (reference 6) and Prandtl's experiments (reference 7) have shown that for a certain - i.e., critical - Reynolds Number, the flow very nearly hugs the back of the sphere again (fig. 1c).

The boundary-layer theory links this phenomenon to

the turbulence of the boundary layer. The effect of this process on the resistance of plates placed parallel with the flow direction is known: In the critical range of R the frictional resistance changes from the subcritical laminar flow to the higher supercritical flow for turbulent boundary layer. The reason for this lies in the strong energy exchange between adjacent layers through intermingling in the turbulent flow. In this manner the boundary layer exerts a marked effect on the external flow.

Conversely, in the case of the sphere the turbulent boundary layer is actuated more forcefully by the outside flow, thus enabling it with a larger volume of motion energy, relative to the laminar flow, to attack the pressure rise starting from the sphere equator. The point of separation at the back of the sphere moves downstream (fig. 1c).

In the critical range of R the pressure prevailing at the back of the sphere rises from negative subcritical (relative to undisturbed flow) at around 0.32 q, to positive supercritical: 0.2 to 0.3 q (fig. 2). The drag coefficient c_w drops correspondingly from about 0.47 to 0.6-0.10 (fig. 13). The breakdown of flow starts, subcritically, slightly upstream from the equator. Starting at this point the flow filaments move tangentially away from the sphere. Supercritically, the flow proceeds largely according to potential theory.

The arguments advanced concerning the boundary layer of the sphere apply, fundamentally, to a number of other interference bodies, such as circular cylinders (reference 8) and airship hulls (reference 9). Bodies whose profiles reveal sharp edges, are little responsive to Reynolds Numbers. Thus on a disk as in figure 1a, the break in pressure to be overcome between the edge and the back of the disk is so sharp and great that the boundary layer is in no case able to overcome it, making it immaterial then whether the boundary layer is turbulent or otherwise.

From among the large number of reports published on sphere measurements, the most important are:

1912 Eiffel (reference 6)

1914 Prandtl and Wieselsberger (references 7 and 10)

1922 N.A.C.A. (reference 11)

1930 Bureau of Standards (reference 12)

1932 Göttingen (reference 14)

1932 A.R.C. (reference 9)

1933 GALCIT (reference 15)

2. EFFECT OF SUSPENSION ON SPHERE DRAG

a) Effect of Rear Support Methods

Experiments in the United States (reference 11) and at Göttingen (reference 3) have revealed the marked effect of the methods of support which interfere with the sphere in its equatorial zone and at its front, on the critical Reynolds Number and the supercritical resistance. The best method of support, interfering least with the flow, is that of the rear mounting spindle, because the rod approaches the sphere at a point where the flow breaks down in either case and is separated anyway, while the sound, outer flow is not touched.

Lacking adequate data on the permanent effect of rear support methods, several experiments were made in the Braunschweiger wind tunnel (reference 17).

The sphere drag was measured by a special arrangement. A scale beam was fitted above the jet, one rod extending vertically into the jet. At its lower end the rod was bent at right angles, approaching the sphere from the rear. Scale beam, rods, and the piece leading to the sphere were completely shielded with pasteboard and sheet metal, so that the pure sphere drag (without support) was measured.

A hollow copper sphere, 25 cm in diameter, was used to explore the effect of varying modifications in support method on the drag in the critical Reynolds range (fig. 5):

1. The diameter of the spindle was increased from 2 to 5 cm by means of a metal sleeve, which resulted in a perceptible drop of supercritical drag;

2. An oblique rod mounted from the rear, radially to the sphere in the air space and extending as far as the surface of the sphere. The super-

critical drag increases considerably, depending on the rod diameter. Thus the oblique spindle disturbs the flow pattern, while the central spindle actually guides the flow;

3. It was not possible to establish whether wires crossing the zone behind the sphere affect the drag curve within instrumental accuracy, or its shape in general. Thus a radial cross of 2.2-millimeter gage wires fitted 8 cm aft of the sphere, disclosed a drag identically the same as with the simple set-up;

4. Extending the shielding of the scale rods forward toward the sphere, up to within 8 cm of its back, lowers the supercritical drag similarly to the reinforced central spindle;

5. The above-cited artifices had no noticeable effect on the subcritical resistance;

6. None of the tests disclosed any effect on the transition from subcritical to supercritical range. It is only when c_w drops below 0.2 that the guiding effect of the central spindle or the disturbing effect of the oblique rods becomes noticeable.

This fact is important for turbulence measurements on spheres.

b) Effect of Spindle Diameter on Supercritical Resistance

In subsequent tests the spheres were threaded into a rear spindle, as shown in figure 4, the spindle itself being suspended from steel wires of 0.4 and 0.7 mm diameter. Owing to the mechanical arrangement, the horizontal force is deflected vertically and measured on a beam scale. Initial tension and calibration is afforded by a wire running rearward over a pulley. The air resistance of the suspension was about 1/8 subcritically, and about 2/3 of the sphere resistance, supercritically.

Experiments were made on a 15-centimeter sphere with support spindles ranging in thickness from 1 cm (original thickness) to 2, 4, and 6 cm, by means of metal sleeves.

When removing the sphere from the spindle with the object of establishing the air resistance of the suspension with blanketed sphere, air forces become effective on the exposed surfaces of sphere and spindle. The manner in which these forces are to be allowed for on thick spindles when computing the sphere drag, must be analyzed. In the present tests the sphere drag was simply defined as the difference of total drag (sphere + suspension) and the resistance due to the suspension. The thus-obtained sphere resistance is that existing in absence of the sphere when the flow pattern remains the same as when the spindle is present. The static pressure on the exposed rear part of the sphere would then be the same as that existing at the front of the spindle. These forces cancel in the calculation, having, referred to sphere resistance, opposite signs.

The results of the tests with divers spindles are as follows (see fig. 5):

1. Agreeable to the arguments in a preceding section, the rear spindle has no traceable effect in the subcritical resistance range;

2. The effect of the spindle on the entry to the supercritical zone is practically nil, except for the thickest spindle (exceeding 1/3 of the sphere diameter) which seems to usher in the transition a little earlier;

3. The effect of the different rear spindles on the supercritical resistance, on the other hand, is marked; the drag coefficient drops by more than 50 percent.

The D.V.L. has also made some corroborating tests by another method. A 15-centimeter steel sphere was suspended from the top by two V wires as a pendulum into the jet of the 1.2-meter wind tunnel (reference 18). Spindles of varying diameter were fitted downstream from the sphere, but separate from it. The axis of suspension of the pendulum was moved toward the air stream by means of a lathe support, until the sphere was released from the spindle. The amplitude of the deflection affords the sphere drag. However, this method is not very accurate because the sphere is subject to marked drag variations and lateral oscillations (±5 percent).

Figure 6 illustrates the effect of the spindle versus the supercritical sphere drag (for temporarily defined Reynolds Number). The fact that the resistance in the D.V.L. tests is twice as high as in the Braunschweig tests, is attributable to the pendulum wires with their well-known interference on sphere flow (references 3 and 11).

A spindle of $d = 1/10\ D$ diameter lowers the supercritical resistance by 12 to 18 percent. The large diameters of the order of $d = \frac{1}{2}\ D$ were for the purpose of ascertaining the further shape of the curve; the drag drops to about 1/4 - the same drag decrease by two different methods. Two values each from figures 3 and 12 fit also into the curves. For supercritical drag measurements. figure 6 stipulates a spindle of minimum diameter ($d = 0.06\ D$?).

As explanation of the effect of spindle/sphere the following is proffered:

1. A thick spindle shortens the theoretically expected pressure rise (fig. 2) at the back of the sphere;

2. The effect of the spindle is approximately equivalent to a tapered offset (streamline form). The flow soon clings to it and removes the piled-up boundary-layer portions profitably.

3. The development and transverse travel of larger vortices is influenced by a spindle, and consequently effects a change in flow pattern.

3. WIND TUNNEL TURBULENCE FROM SPHERE MEASUREMENTS

a) Concept of Turbulence

In a great many cases the turbulence of the air stream in a wind tunnel affects the magnitude and course of the air forces. For instance, the maximum lift of a wing is, as is known, markedly affected by the turbulence. For this reason, the knowledge of the turbulence existing in a wind tunnel is necessary.

The concept "turbulence" is ambiguous to the extent that the individual "turbulence balls" formed through

jointly circling or oscillating motion of air particles, may be unlike in extent (diameter) as well as in sequence. Rough disturbances in free atmosphere are known by the name of gusts. But such do not occur in the tunnel flow because it is guided and straightened. Even so, the flow is more or less interspersed with fine vortices having diameters of the order of 1 cm which, as is known, act upon the boundary layer of bodies exposed to it.

And it is of this effective turbulence of the boundary layer that we shall speak hereinafter. The type of turbulence is accordingly characterized by its effect without it being necessary to know anything concerning its nature or mechanism. Yet, obviously, the turbulence is matched by certain pressure and speed fluctuations of the flow; and these were measured and recorded in the U.S. by hot-wire anemometer and oscillograph (references 19 and 12). Detailed information about the process of turbulent motion or the magnitude of the oscillating air balls is not given in these measurements.

b) Test Procedure

From the arguments advanced about the boundary layer of the sphere in a previous section (1b, p. 4), it is clear that in the zone directly below the critical Reynolds Number, the transition to supercritical flow is prematurely induced by the turbulence already existing in the utilized flow. Thus the Reynolds Number at which the drag of a test sphere drops to the supercritically lower figure is a criterion for the boundary-layer effective turbulence dwelling within the flow. This possibility has been frequently resorted to for comparative turbulence measurements in the wind tunnel. Customarily that Reynolds Number is given as critical for which the drag coefficient $c_w = 0.3$. The connection between the critical R of the sphere and the air-speed fluctuations is shown in figure 7.

The use of the sphere as indicator of the turbulence, originally proposed by Professor Prandtl in 1914 (reference 7), has the marked advantage from the point of view of wind-tunnel practice, in that it indicates the effect of turbulence on a body directly.

As previously pointed out, the method of support, so far as it approaches the sphere from the rear, has no effect in turbulence measurements. Contrariwise, the degree

of surface roughness of the test sphere affects the critical velocity to the same approximate amount as the turbulence of the flow, for which reason the sphere must be of accurate design and perfectly smooth surface if used for turbulence measurements.

c) Turbulence at Various Speeds

From sphere measurements of different diameters made in the Braunschweig as well as in the 1.2-meter tunnel of the D.V.L., it is known that the critical Reynolds Numbers for large spheres are perceptible lower than for small spheres. For the Braunschweig tunnel, figure 8 gives the critical R (times 10^5) and speeds v_k as follows:

Without honeycomb	9	cm	sphere	R_k =	2.52	v_k =	39 m/s
	15	"	"	"	2.25	"	21 "
With honeycomb	9	"	"	"	3.18	"	49 "
	15	"	"	"	2.95	"	29 "

The data for the 1.2-meter tunnel of the D.V.L. were:

15 cm steel sphere	R_k =	3.50	v_k =	34 m/s
Polished 28 cm silumin sphere	"	3.20	"	17 "

The few known tests on spheres of varying diameter from other wind tunnels repeatedly disclose the critical Reynolds Number for large spheres to be lower than for small ones as, for example (reference 12), with the 5- and 8.6-inch sphere in the 10-foot tunnel and, more recently, (reference 15), for four different sphere diameters, as illustrated in figure 9.

There being no doubt about the validity of Reynolds law for the critical range of the sphere, the conclusion is, that the degree of turbulence at different tunnel speeds used for spheres of different diameters, is varying. Patently, the effective turbulence in all tunnels, cited in figure 9, is greatest at low speeds; it decreases perceptibly with the speed. Defining from the calibration curve of figure 7, the speed fluctuations on which the turbulence is based, it is found that in the 1.2-meter D.V.L. tunnel and in the Pasadena tunnel, they decrease from 0.3 percent at low speeds to 0.1 percent at high speeds.

The incongruity of the transition curves of various sizes of spheres should disappear in towing tests in still water because of the absence of turbulence. The published reports of Krey (reference 22) and Eisner (reference 23) on spheres and cylinders do not adduce the expected proof, since in both, the boundary layer is disturbed at a sensitive point as a result of the support method employed.

From the above, it seems advisable when comparing turbulence measurements of different tunnels, to take the sphere diameter and the critical speed range into consideration. For instance, a sphere having a diameter such that the critical transition takes place within the occasional speed range of normal model tests, could be used. From the point of view of wind-tunnel practice, figure 9 possibly postulates that the speed should be high when the turbulence is low.

d) Comparison of Different Wind Tunnels

Figure 10 gives the sphere tests from other wind tunnels plotted in the usual double logarithmic form. The Braunschweig and D.V.L. tests are in exceptionally close agreement with the Göttingen curves (reference 14) both as to subcritical and supercritical resistance as well as to transition.

It is generally conceded that contraction of the flow section insures very uniform test streams (reference 24, p. 73). Quite obviously, such contraction lowers the turbulence of the flow in the same manner as local speed discrepancies are compensated. In figure 11 the critical Reynolds Numbers representative of the turbulence have been plotted against the contraction ratio of the tunnels as established for the sphere in the different wind tunnels.

In two instances, values are given for the same tunnel but for different nozzle length; that is, unlike contraction ratios. In the 1.2-meter tunnel of the D.V.L. an extra nozzle was fitted which narrowed the nozzle section from 1.13 to 0.2 m^2. The critical R recorded with this 22:1 contraction ratio $R_k = 3.53 \times 10^5$ (fig. 12) approaches $R_k = 3.72 \times 10^5$ obtained with the same sphere in air free from turbulence (section 5).

TABLE I

Sphere turbulence tests; the turbulence corresponds to the critical Reynolds Number $R\ 10^5$
Contraction ratio $f = F_o/F$

No.	Wind tunnel	Features	f	R_k (10^5)	Source (reference)
1	D.V.L. 1.2 m	without honeycomb	4.0	2.6	-
2	" "	with honeycomb	4.0	3.2	-
3	" "	with extra nozzle	22.0	3.5	-
4	" "	with extra nozzle, corrected	22.0	3.8	-
5	" "	smooth 15 cm sphere	4.0	3.5	-
6	" "	status, 1935	4.0	3.6	-
7	Göttingen, large	with honeycomb	5.0	3.2	14
8	" small	" "	2.1	2.8	14
9	Göttingen, propeller research	small nozzle	6.2	3.1	14
10	Göttingen, propeller research	large nozzle	2.8	2.4	14
11	Braunschweig	without honeycomb	4.8	2.4	-
12	"	with honeycomb	4.8	3.0	-
13	N.A.C.A. variable density	closed (1925)	1.0	0.9	11
14	N.A.C.A. variable density	open jet (1929)	2.5	1.6	13
15	N.A.C.A. variable density	closed (1930)	1.0	1.2	13

TABLE I (Cont.)

No.	Wind tunnel	Features	f	R_k (10^5)	Source (reference)
16	N.A.C.A. tunnel No. 1	with honeycomb	3.1	1.7	21
17	N.A.C.A., vertical	free jet without	3.2	1.8	28
18	N.A.C.A., full-scale	jet center for the rest	5.0	3.4	16
19	N.A.C.A., full-scale		5.0	3.7	16
20	Bur. Standards, 10-foot	long approach	1.0	2.3	12
21	Bur. Standards 4.5-foot	short approach	1.0	1.7	12
22	Bur. Standards 3-foot		5.5	2.7	12
23	GALCIT, Pasadena	without honeycomb	4.0	3.3	15
24	M.I.T., 7.5-foot	N.P.L. type	1.5	2.1	9
25	M.I.T., air	towing test	-	2.9	26
26	Akron, Guggenheim	vertical, free	4.2	2.6	29
27	N.P.L., variable pressure	no data	-	1.9	30
28	Turin	N.P.L. type	4.5	2.0	31
29	D.V.L., free air	flight and towing test	-	4.0	-
30	GALCIT, free air	flight test	-	3.7	15

Figure 11 shows how the quality of the tunnels from the point of view of turbulence, increases with the con-

traction ratio. Admittedly, the turbulence established in the test section is not merely contingent upon the contraction, but very considerably also on the quality of the flow upstream from this contraction (disturbances due to fan, enlargement, directional changes). Another governing factor is the length of the steady flow area in front of the nozzle contraction.

In highly turbulent tunnels the critical Reynolds Numbers range at $R \approx 1.0$, for good tunnels of the earlier English type (without substantial contraction, long entry) $R_k = 1.7$ to 2.3, for good tunnels of the Gottingen type (contraction 4 to 5:1), $R_k = 3.0$ to 3.5, and for nonturbulent air (section 5) $R_k = 3.7$ to 4.1×10^5. The measurement in the 1.2-meter tunnel of the D.V.L. (status 1935) excels, with $R_k = 3.6$, all other wind-tunnel values known at the present time.

4. WIND-TUNNEL TESTS ON TURBULENCE

a) Critical Reynolds Number by Pressure Method

According to section 1, the pressure distribution changes the sphere drag. Consequently, it is very natural to observe the pressure at the back of the sphere by the simple expedient of using the sphere as a turbulence indicator. This pressure must, in conformity with the drag coefficient, pass through a critical value.

The procedure of measuring the pressure at the back of the sphere is as follows: The sphere is screwed into a rear tube having four holes where it touches the surface of the sphere so that the static pressure existing in the angle between sphere and tube is carried through the spindle.

Figure 13 shows the drag and pressure for two spheres plotted against the same Reynolds Number. The pressure curve $(p_{r\ddot{u}}/q)$ is the reflected drag curve (c_w). The connection between $p_{r\ddot{u}}$ and c_w is accurately established through concurrent measurement and plotted in figure 14. Although the curve is, strictly speaking, valid only for the perfectly smooth 15-centimeter sphere in nonturbulent flow $(R_k = 3.6 \times 10^5)$, it may, nevertheless,

be presumed that in turbulent flow, for instance, the same relation exists between c_w and p''_{ru}. In the graph the test points range themselves below the curve computable from the pressure distribution. This discrepancy has not been cleared up.

The critical Reynolds Number is, conveniently, that for which the pressure at the back of the sphere changes from negative subcritical to positive supercritical; that is, where $p''_{ru} = 0$. The thus-defined figures are slightly higher (about 2 percent) than those obtained for $c_w = 0.3$.

The critical dynamic pressure q_k is very accurately defined in the measurements. A 1-percent change in q_k, either upward or downward, causes p''_{ru} to deflect about 8 percent from zero, so that even the least differences in turbulence are sharply recorded. The pressure method obviates the cumbersome sphere drag measurement. It suffices to find the dynamic pressure at which $p''_{ru} = 0$; R_k is therefore obtained with one single test point.

b) Turbulence Due to Individual Wires

In many instances it is advisable to use turbulence grids in wind-tunnel tests; that is, in cases when, through generation of artificial turbulence, critical zones of Reynolds Numbers (as on an airplane wing, for example) are skipped and precritical conditions are avoided. (See reference 32, p. 188.) To supply data for such turbulence grids with respect to wire thickness and wire spacing, the D.V.L. explored the vortex streets of individual wires, using the sphere as turbulence indicator.

Figure 15 illustrates the effect of various gage wires stretched, exactly centered, across the jet at a number of distances upstream from the sphere. The thicker the wire is, the lower the critical dynamic pressure becomes.

The wire turbulence exerts at first a startling effect on the supercritical sphere pressure p''_{ru}, according to figure 15. Small gage wire (about 1 mm) causes the pressure, at first, to rise to +0.37 q. According to

that, the insertion of a thin wire must lower p_{ru}. The effect of thin wires was also the same at substantially higher R. An explanation for this might be found in the fact that a single wire makes one certain plane of the flow turbulent and thus influences the arrangement of the vortices in the wake of the sphere.

The growth in supercritical sphere drag (corresponding to the abatement of rear pressure) due to enhanced turbulence (thicker wires) is attributable to the "apparently" greater viscosity of the moving air caused by turbulence. The apparent viscosity effectuates supercritically a boundary-layer lag similar to that known subcritically through actual viscosity. This fact is important for the application of turbulence grids in model tests. To be sure, an artificial turbulence creates a "supercritical" condition. But this condition is unlike that afforded by increasing the Reynolds Number because of greater effective viscosity of the flowing fluid; that is, a third condition is reached.

Figure 16 shows the turbulence effect of various wires mounted at varying distances upstream from the sphere. Right next to the sphere the effect is small; evidently the much lower flow velocity at that point (indicated in fig. 16) permits no large vortices. Similar experiments with turbulence grids may be found in reference 9.

The effect of the lateral position of the turbulence wires on the sphere (fig. 17) is indicative of the spatial expansion of the vortex streets aft of the wires. Thin wires in particular (1 mm) have an expressed directional effect. The very fact that this effect disappears almost altogether when moved a millimeter away from the sphere axis, proves the importance attached to the introduction of turbulence into the boundary layer through the exact stagnation point. Thicker wires have a substantially more expansive vortex street whose turbulence then also penetrates the boundary layer of the sphere when the wires are placed laterally from the sphere axis.

Figure 18 depicts the turbulence effect of two parallel wires. At a certain short distance their effect is comparatively small. Ostensibly, the adjacent inner sides of the vortex streets emanating from the wires cannot really develop.

As the distance is increased, the ensuing turbulence reaches a maximum (q_k reaches a minimum). Upon still farther removal the effect of the wires disappears because the vortex streets produced by them pass externally on the sphere.

c) Effect of Acoustic Air Vibrations on Boundary Layer

According to experiments in the United States with hot wires (references 19 and 15), the critical Reynolds Number observed on a sphere is definitely tied to the speed fluctuations of the flow forming the turbulence (fig. 7). This seems to indicate that the effect of acoustic air vibrations on the boundary layer of a moving body is the same as that of the measured speed fluctuations. In order to clear up this point, various spheres were exposed to a loud whistling tone and observed.

The tone of around 3,000 Hertz was supplied from a steam whistle (1.5 to 3 atm. at the whistle) through a funnel mounted obliquely 1 meter upstream from the sphere. Figure 19 gives the pressure of the 15-centimeter sphere. For the rest, the critical Reynolds Numbers for the whistling tone (figures without tone given in brackets) are as follows:

28 cm sphere $R_k = 3.04 \times 10^5$ (3.13)

15 " " $R_k = 2.40 \times 10^5$ (3.50)

7 " " $R_k = 2.74 \times 10^5$ (3.24)

The tone affects all three spheres; the R_k are reduced from 3 to 31 percent. The acoustic interference of the boundary layer is similar to that of the turbulence grid. The 28-centimeter sphere has the least tonal interference; its R_k changes fairly little. For the 7-centimeter and 15-centimeter spheres the effect of the acoustic vibrations is marked. The oscillation frequency (3,000 Hz) is perhaps better suited to the smaller spheres than to the large one or, better fitted to the high than to the low speeds.

The boundary-layer effect of the acoustic oscillations was also observed experimentally on a model airplane wing; the maximum lift change was negligible.

According to present-day experimental data, a boundary-layer effective wind-tunnel turbulence is caused by

1. Rough interference of tunnel flow due to enlargement, faulty directional changes, etc.;

2. Vortex streets emanating from honeycomb walls, deflector vanes, and turbulence grids;

3. Air oscillations (audible) which correspond to the blade strokes of the fan. Such oscillations have been previously recorded (reference 25).

5. TURBULENCE TEST IN FREE AIR

a) Generalities

On the subject of boundary-layer effective turbulence in free air, the following sphere tests have been published:

In 1922 the N.A.C.A. made a series of drop tests from great altitude in which the drag forces and the speed were measured (reference 11).

In the 1932 flight tests at Pasadena, the sphere was fitted on the airplane while the drag forces were recorded with a special hydraulic instrument.

In the 1934 tests at Pasadena, a large sphere was towed in a closed hangar (reference 26). The drag was recorded by an instrument fitted to the sphere.

In view of the wide divergence of critical Reynolds Numbers in the first two experiments, the D.V.L. decided in 1933 to make its own sphere tests in free air. The aim of these tests was to establish the critical Reynolds Number in air free from turbulence, with a view to obtaining a criterion - a "zero point" for the tunnel turbulence tests and to measure that turbulence in free air, which may be anticipated as boundary-layer effective turbulence on a real airplane.

b) Test Procedure

Weighing of air resistance was abandoned in favor of pressure measurement as described in section 4a. It is a particularly advantageous method for flight testing where the installation of scales is very difficult, whereas pressure measurements may be made quite simply.

The sphere is screwed into a rear spindle, pivoted on a small mast, and fitted with guide vane, as shown in figure 20. The mast was first mounted on a towing car and subsequently fitted on top of an airplane, as shown in the photograph.

The dynamic pressure q is recorded through the orifice in the front of the sphere. The pressure p_{ru}'' at the back of the sphere, is recorded in the bend between sphere and spindle, while the static back pressure p_o is measured on the spindle about 4 sphere diameters aft of the sphere but upstream from the guide vane. It was found from wind-tunnel tests that the static pressure downstream from the sphere returned very soon from its negative (subcritical) or positive (supercritical) to that of the p_o value corresponding to undisturbed flow. Subcritically, this takes place at a distance of about $3\frac{1}{2}$ sphere diameters from the back of the sphere, supercritically, after $2\frac{1}{2}$ diameters already.

The flight tests revealed that the pressure field of the airplane mostly evinced a value at the place of the sphere which was slightly unlike that at the more rearwardly located test station for p_o. The pressure difference was established for different flight speeds and flight conditions (full throttle and gliding) by comparison of $p_{spindle}$ with a static pitot tube mounted in place of the sphere. The sphere records were corrected conformably to the calibration curves.

The airplane was a Junkers type W 34, powered with an SH-20 engine; speed range, 56 to 130 m.p.h. The automobile was an old-type touring car having a speed of 52-53 m.p.h. The Reynolds Numbers were obtained from temperature and air-pressure readings (with sensitive altimeters in flight tests). The pressures were recorded on two Askania differential manometers. These recording instruments, fitted with soft metal capsules, are especially

practical for readings on disturbed points. They are simple to read, sensitive, and free from inertia to within 2 percent; and fairly insensitive to location and acceleration.

The records for two spheres are shown in figures 21 and 22: Subcritical, both curves follow the parameter $p''_{ru} = -0.32\ q$ measured in the tunnel; supercritical, the curves range within $p''_{ru} = +(0.25 \text{ to } 0.30)\ q$. The free-air tests are plotted in figure 23, while figure 24 illustrates the data for the same spheres as obtained in the 1.2-meter tunnel of the D.V.L.

c) Surface Roughness

The 28-centimeter silumin sphere shows the highest Reynolds Number in air free from turbulence according to table II. These spheres of identical manufacture (silumin casting, expertly machined and polished with shellac) have about the same degree of surface roughness. Owing to the fact that the remanent surface roughness on small spheres appears greater relative to sphere diameter, it may be inferred that this very roughness induces lower critical Reynolds Numbers than on larger spheres. Being relatively the smoothest, the 28-centimeter sphere shows as maximum, $R_k = 4.03$.

TABLE II

Critical $R(10^5)$ of Different Spheres in Free Air

Sphere	Still, free air	Moving air	1.2 m tunnel
7 cm silumin	full throttle, 3.48	-	3.38×10^5
14 cm silumin	full throttle, 3.72	-	3.27×10^5
28 cm silumin	automobile, 4.03	street, wind 2.70	3.20×10^5
15 cm steel	full throttle, 3.92 gliding, 4.00	rough weather 3.85 airport, 3.60	3.50×10^5

Based on this turn of the results, the 15-centimeter sphere was prepared and flight-tested. It is the ball bearing described in section 6. The R_k obtained with it is fairly the same as that for the 28-centimeter sphere.

In view of the almost perfect polish of the silumin spheres, the influence of the surface roughness on R_k was observed to be unusually pronounced. It is likely that a carefully polished sphere safeguarded against oscillations reaches R_k values even higher than those obtained in the present experiment; the extrapolation in figure 25 seems to point toward 4.1.

d) Results

The experiments with the 15-centimeter steel sphere ranged over a series of flight tests at altitudes of 6,500 to 13,125 feet in level flight, climb at full throttle, and glide power-off under various weather conditions, in which the critical dynamic pressure (at which $p''_{ru} = 0$)

and the correlated R_k were determined.

There is no systematic change of R_k with altitude, etc., as far as we could ascertain. The critical figures for the atmosphere ranged between 3.85 and 4.05 $\times 10^5$; the figures for the glide are, on the whole, 0.1 higher than for flight with full throttle. An explanation for this is looked for in the engine vibrations.

The value for full throttle in gusty weather was $R_k = 3.85$, or in other words, the boundary-layer effective turbulence in squally weather is very small. The tests with the open touring car in still air disclosed $R_k = 4.03 \times 10^5$; for the tree-bordered street in side wind it dropped to $R_k = 2.7 \times 10^5$, on the airport surrounded by buildings (16 feet over the ground) with wind, it was $R_k = 3.6$. Consequently, there is a boundary-layer effective turbulence behind obstacles in the boundary layer of the earth's surface. This fact conforms with the Pasadena flight tests (reference 15), with $R_k = 3.68$ in calm weather, and $R_k = 3.45$ in storm a few feet above ground.

The discrepancy of the Pasadena data from those of the D.V.L. is probably due to the sphere which they used. More recently published data (reference 26) for a large rubber sphere towed in a closed hangar, show $R_k = 2.9 \times 10^5$.

The N.A.C.A. drop tests (reference 11) were made with large spheres and, of course, without engine vibrations. (Steady condition in free drop? Variable air density?) If the test points plotted in figure 10 are to reveal a critical Reynolds Number, it would possibly lie between 4 and 5 $\times 10^5$.

6. SURFACE ROUGHNESS TESTS

a) Effect on R_k

It is a well-known fact that the surface roughness in pipes and on flat walls favors the transition from laminar to turbulent boundary-layer flow quite considerably. It is therefore, self-evident, according to section 1b, that roughness or irregularities on the surface lowers the R_k value of the sphere.

The Braunschweig experiments included among others,

hollow copper and sheet brass spheres with fine circular waves and bulges running along the welds. For the rest, they were smoothly polished. In contrast, the steel spheres were exactly round; they were 9-, 12-, and 15-centimeter ball bearings supplied by the Fischer Company of Schweinfurt.

Figure 8 reveals the varied resistance curve of the different spheres. Compared to the steel spheres, those of sheet metal showed the critical transition throughout at perceptibly lower R_k values. Thus, for a 10-centimeter sheet-metal sphere, for instance, it is $R_k = 2.08 \times 10^5$ against $R_k = 2.38$ for the 12-centimeter steel sphere (identical channel condition), and $R_k = 2.52 \times 10^5$ for the 9-centimeter sphere.

On the 25-centimeter sheet-metal sphere, having along its weld in the equator a circular bulge of about 0.4 mm, it was noted that at a certain speed the resistance reveals a sharp break without intermediate stage from subcritical to supercritical, and jumps just as suddenly from supercritical to subcritical again when the speed is the same (fig. 8).

Result: The waviness of the surface induces a substantially earlier critical transition, besides being erratic and at times, discontinuous.

The effect of surface roughness (without waviness) has been explored on cylinders. Unfortunately, the English source (reference 8) does not give the grain texture, thus leaving the degree of questionable roughness unexplained.

In support of the surface roughness in free-air tests inferred from section 5c, we made a number of systematic tests with the 28-centimeter silumin sphere, which had been coated with a shellac solution and sprinkled closely with sand grains of a certain screen size.

Figure 25 discloses the rate at which the R_k value drops with the degree of roughness. The extrapolation to $\frac{k}{D} = 0$ gives approximately $R_k = 4.1 \times 10^5$ for air free from turbulence; this is the R_k value of the perfectly smooth sphere in air free from turbulence applicable to car-test conditions. The plot also includes the data for

different silumin spheres with an estimated roughness of 1/100 or 1.5/100 mm.

b) Relation of the Supercritical Drag

The boundary layer governs the drag even beyond the critical R. The greater its lag on the sphere front, through surface roughness, for example, the higher the form drag.

According to accepted conception, a surface acts aerodynamically as smooth when protuberances in the laminar sublayer of the boundary layer next to the surface, which also exist in the turbulent boundary layer, are wholly imbedded. In fact, it is only by virtue of this premise that supercritical, aerodynamically perfectly smooth spheres can be manufactured. For flat surfaces exposed horizontally to flow, supercritically the permissible grain size or texture becomes consistently smaller with the Reynolds Number. The extreme condition for grain size is the approximately constant $R_{grain} = v \frac{k}{w} = 1.5 \times 10^2$ (reference 27). The end resistance then in the turbulent rough friction is constant in relation to grain size (squared resistance law).

Supercritically, the resistance curve for the sphere is basically the same as for the plate. The frictional resistance appears "raised to a power" as form resistance, so that c_w should continue to decrease with the Reynolds Number for very smooth spheres (fig. 27a). The technical preparation of surface smoothness necessary at high R (over 5×10^6) should prove very difficult. The grain of the 28-centimeter sphere would then have to be considerably smaller than 1/10000 mm. As figure 27 indicates, rough spheres reach, supercritically, a certain end resistance, as actually recorded in the variable-density wind tunnel (fig. 10). Adequately rough spheres never leave the subcritical flow pattern according to figure 26 ($\frac{k}{D} = 0.004$), so that the c_w, supercritically, with about 0.47 also may be assumed constant (fig. 27d). Spheres with such a degree of roughness are, therefore, insensitive to R; the separated subcritical flow is not abandoned when its boundary layer becomes turbulent.

The remarkable fact is, that for a given surface, the

turbulence increases the supercritical resistance three times as high (fig. 28). This may, on the one hand, be attributable to apparently intensified viscosity, while on the other hand, the permissible grain size is, without a doubt, smaller in turbulent flow. On the premise of smooth surface, the criterion for turbulence is, accordingly, not only the R_k value but also the supercritical resistance. In fact, it seems one-sided to confine always the investigation to the influence of turbulence on the R_k value. The majority of flow processes are supercritical, whence it is very desirable to know what supercritical effect the turbulence has.

c) Application to Wind-Tunnel Tests

The R_k values obtained for the various spheres in air free from turbulence may be considered as calibration for "turbulence = 0" for these spheres. The lower the wind-tunnel figures below those for free air, the greater the wind-tunnel turbulence. According to figure 25, it is possible to extrapolate to $\frac{k}{D} = 0$, when the free-air figure for a sphere is known. If, due to roughness, the R_k value of a sphere in free air is 10 percent lower, the figure measured in turbulent flow will be too low by about the same percent.

Figures 9 and 11 show the values corrected in this manner according to figure 25. Thus, the corresponding curve in figure 9 gives the Reynolds Numbers which would be obtained at different air speeds, with perfectly smooth spheres (of varying diameters). The decrease of turbulence with the tunnel speed is so great for the explored tunnels that through it the influence of the relatively greater roughness on small spheres is exceeded.

As regards turbulence and surface roughness the sphere-drag tests should be interpreted, according to figures 27 and 28, as follows:

1. Roughness shifts the resistance break toward lower Reynolds Numbers, although the transition takes place equally steep (fig. 27c);

2. Turbulence also forces a premature break, although the transition curve is, inherently, flatter (fig. 28b);

3. Supercritically, the drag coefficient for smooth spheres drops consistently (fig. 27a);

4. This should hold true for turbulent flow as well; although the curve lies higher, the permissible roughness is less (fig. 28b);

5. Roughness prevents a temporary drop in supercritical drag (fig. 27b); with sufficient roughness the drag increases again until it reaches the constant supercritical end drag (fig. 27c);

6. There is no critical resistance break when the roughness is coarse; c_w remains at around 0.47. Like all bodies having sharp edges, the sphere is then insensitive to Reynolds Number (fig. 27d).

Translation by J. Vanier,
National Advisory Committee
for Aeronautics.

REFERENCES

1. Muttray, H.: Die experimentellen Tatsachen des Widerstandes ohne auftrieb. Handb. Exp. Phys. Wien Harms, Bd. IV 2, S. 232, 291.

2. Hoerner, S.: Untersuchungen Windkanal, T.H. Braunschweig. Diss. Braunschweig, 1933.

3. Flachsbart, O.: Recent Researches on the Air Resistance of Spheres. T.M. No. 475, N.A.C.A., 1928.

4. Prandtl, L., and Betz, A.: Ergb. Aero. Vers. zu Göttingen, II Lieferung, 1927.

5. Prandtl, L., and Betz, A.: Ergb. Aero. Vers. zu Göttingen, III Lieferung, 1929, p. 6.

6. Eiffel, G.: Récherches résistance de l'air et l'aviation, Paris, 1914.

7. Prandtl, L.: Nachr. Ges. Wissensch. Göttingen, math. phys. Kl. 1914.

8. Fage, A., and Warsap, J. H.: The Effects of Turbulence and Surface Roughness on the Drag of a Circular Cylinder. R. & M. No. 1283, British A.R.C., 1930.

9. Lyon, H. M.: Effect of Turbulence on Drag of Airship Models. R. & M. No. 1511, British A.R.C., 1933.

10. Wieselsberger, C.: Luftwiderstand von Kugeln. Z.F.M., May 16, 1914, S. 140.

11. Bacon, D. L., and Reid, E. G.: The Resistance of Spheres in Wind Tunnels and in Air. T.R. No. 185, N.A.C.A., 1924.

12. Dryden, H. L., and Kuethe, A. M.: Effect of Turbulence in Wind Tunnel Measurements. T.R. No. 342, N.A.C.A., 1930.

13. Jacobs, Eastman N.: The Aerodynamic Characteristics of Eight Very Thick Airfoils from Tests in the Variable Density Wind Tunnel. T.R. No. 391, N.A.C.A., 1931.

$.004 \times 2m = .008m = 8mm = \frac{8mm}{25.4\frac{mm}{in}} \doteq .32in$

$.0036 \rightarrow .28in$

.05 →

$$\frac{.05}{28} = \frac{1}{20 \times 28} = \frac{1}{560} = .0018$$

$$\frac{.1}{28} = \frac{1}{280} = .0036$$

$$\frac{.4}{28} = = \frac{.1}{7} = .014$$

14. Flachsbart, O.: Der Widerstand von Kugeln in der Umgebung der kritischen Reynolds schen Zahl. Ergb. Aero. Vers. zu Göttingen, IV Lieferung, 1932, S. 106.

15. Millikan, Clark B., and Klein, A. L.: The Effect of Turbulence. An Investigation of Maximum Lift Coefficient and Turbulence in Wind Tunnels and in Flight. Aircraft Engineering, August 1933, p. 169.

16. Silverstein, Abe: Scale Effect on Clark Y Airfoil Characteristics from N.A.C.A. Full-Scale Wind-Tunnel Tests. T.R. No. 502, N.A.C.A., 1934.

17. Hoerner, S.: Der Windkanal im Flugtechnischen Institut der TH Braunschweig. Z.F.M., Bd. 23, August 27, 1932, p. 486.

18. Seewald, Friedrich: The Small Wind Tunnel of the DVL. T.M. No. 734, N.A.C.A., 1934.

19. Dryden, H. L., and Kuethe, A. M.: The Measurement of Fluctuations of Air Speed by the Hot-Wire Anemometer. T.R. No. 320, N.A.C.A., 1929.

20. Dryden, H. L.: Reduction of Turbulence in Wind Tunnels. T.R. No. 392, N.A.C.A., 1931.

21. Reid, Elliott G.: Standardization Tests of N.A.C.A. No. 1 Wind Tunnel. T.R. No. 195, N.A.C.A., 1924.

22. Krey: Sandkörner und Kugeln in Wasser. Mitt. Vers.-Anst. Wasserbau Schiffbau, Berlin, 1921.

23. Eisner: Widerstandsmessungen an Zylindern. Mitt. Pr. Vers.-Anst. Wasserbau Schiffbau, Berlin, Heft 14, 1929.

24. Prandtl, L.: Attaining a Steady Air Stream in Wind Tunnels. T.M. No. 726, N.A.C.A., 1933.

25. Doetsch, H., and Mathes, P. v.: Schwankungsmessungen im Windkanal. Abh. a.d. Aerod. Inst. an der Tech. Hochs. Aachen, Heft 10, 1931.

26. Sauerwein, R. T.: Sphere Drag Determined by Coasting through Still Air. Jour. Aeronautical Sciences, July 1934, p. 147.

27. Prandtl, L., and Schlichting, H.: Widerstandsgesetz rauher Platten. Werft Reederei Hafen, vol. 15, no. 1, Jan. 1, 1934, pp. 1-4.

28. Wenzinger, Carl J., and Harris, Thomas A.: The Vertical Wind Tunnel of the National Advisory Committee for Aeronautics. T.R. No. 387, N.A.C.A., 1931.

29. Troller, Theodor: The Vertical Wind Tunnel of the Daniel Guggenheim Airship Institute. The Daniel Guggenheim Airship Institute, pub. No. 1, 1933, p. 11.

30. Relf, Ernest F.: Results from the Compressed Air Tunnel. Jour. Roy. Aeron. Soc., January 1935, pp. 1-30

31. Ferrari, C.: Determinazione delle Caratteristiche della Galleria del Vento (Torino). L'Aerotecnica, vol. XIV, no. 4, 1934, p. 380.

32. Seiferth, R., and Betz, A.: Untersuchung von Flugzeugmodellen im Windkanal. Handb. Exp. Phys. Wien Harms, Bd. IV, 2, 1933, S. 107.

a, Disk
c_w = 1.20

b, Sphere
sub critical
c_w = 0.47

c, Sphere
super
critical
c_w = 0.08

d, Spindle
shape
c_w = 0.04

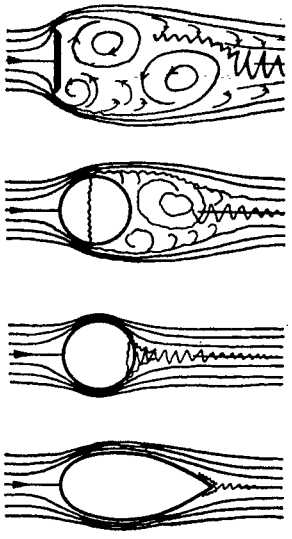

Figure 1.- Flow around various interference bodies.

cm x .3937 = in.

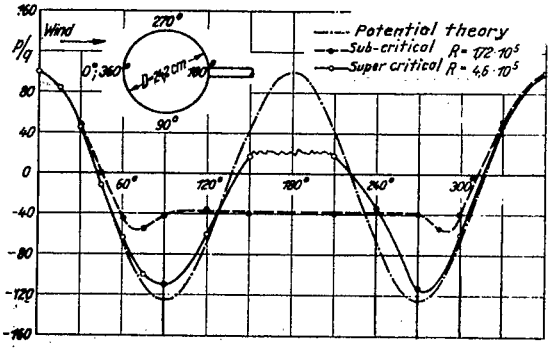

Figure 2.- Pressure distribution over sphere (ref. 3).

Figure 4. Mounting of 15 cm sphere in Braunschweig wind tunnel, the sloping rear wires connect with the scale above the jet.

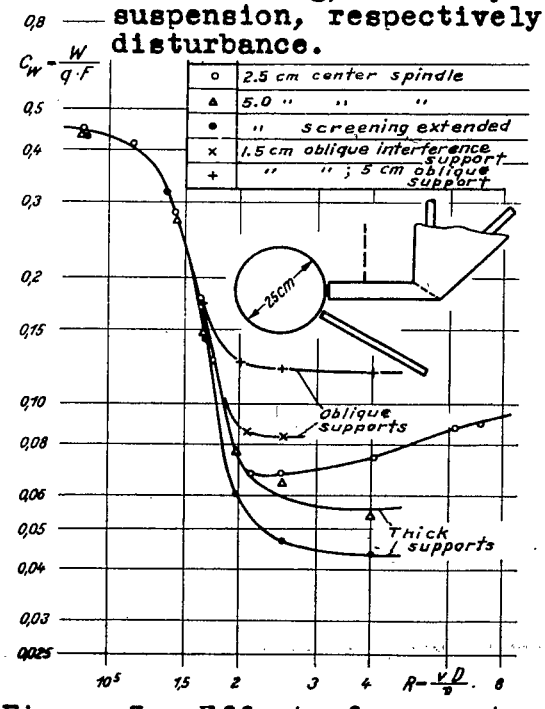

Figure 3.- Effect of support method in the wake of the sphere on its drag.

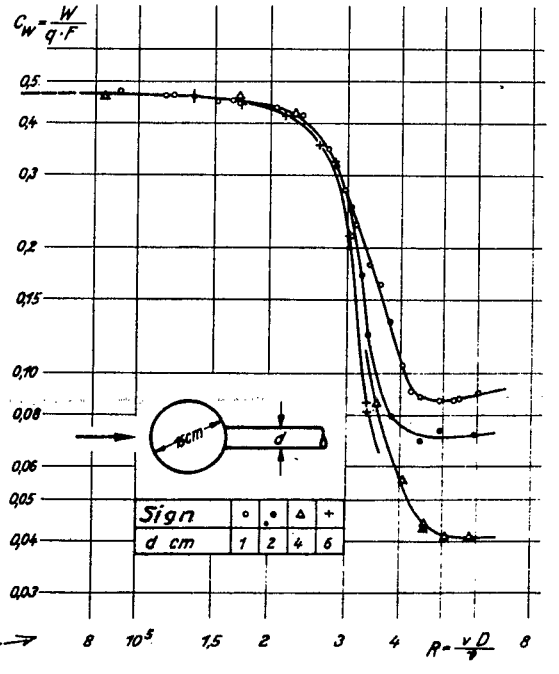

Figure 5. Effect of rear spindle on sphere drag.

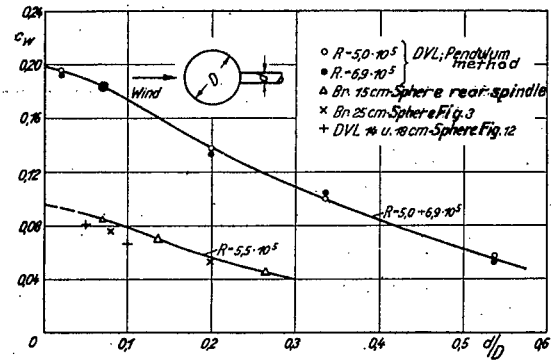

Figure 6.- Super-critical drag of various spheres versus spindle diameter.

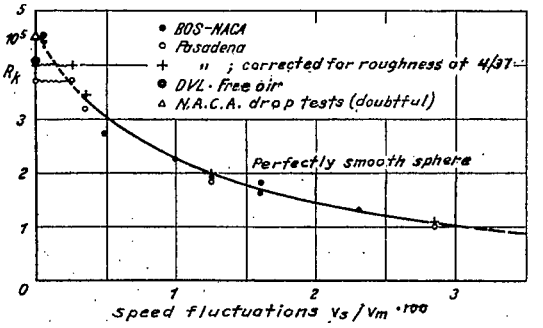

Figure 7.- Critical Reynolds Number versus speed fluctuations.

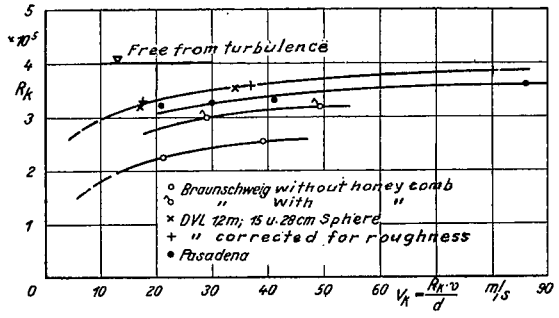

Figure 9.- Turbulence at various air-speeds.

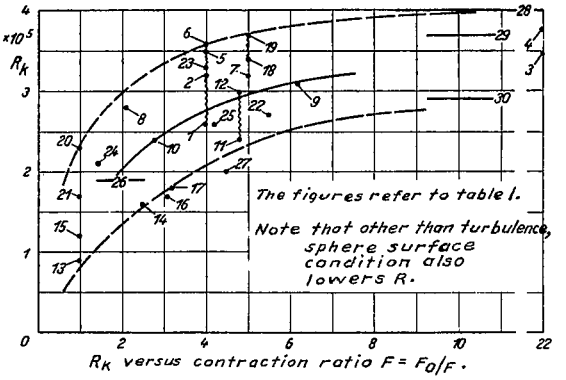

Figure 11.- Effect of channel contraction on turbulence.

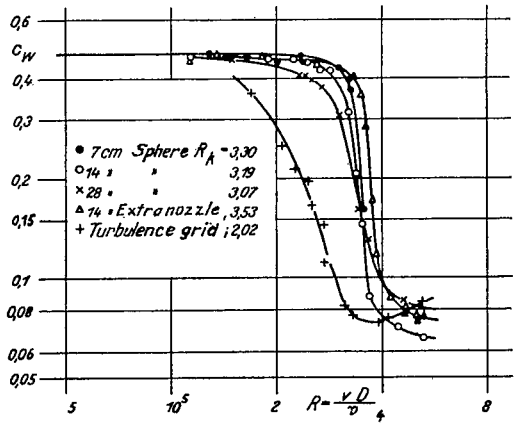

Figure 12.- Sphere drag curves in the 1.2m DVL tunnel.

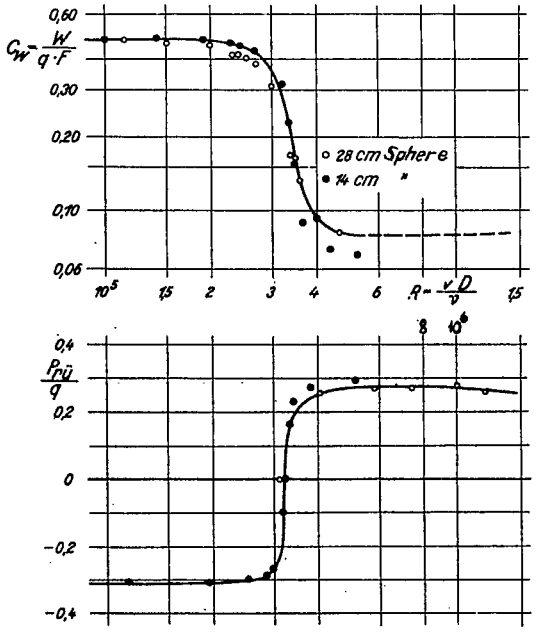

Figure 13.- Drag and pressure at back of two spheres versus R; (DVL tunnel).

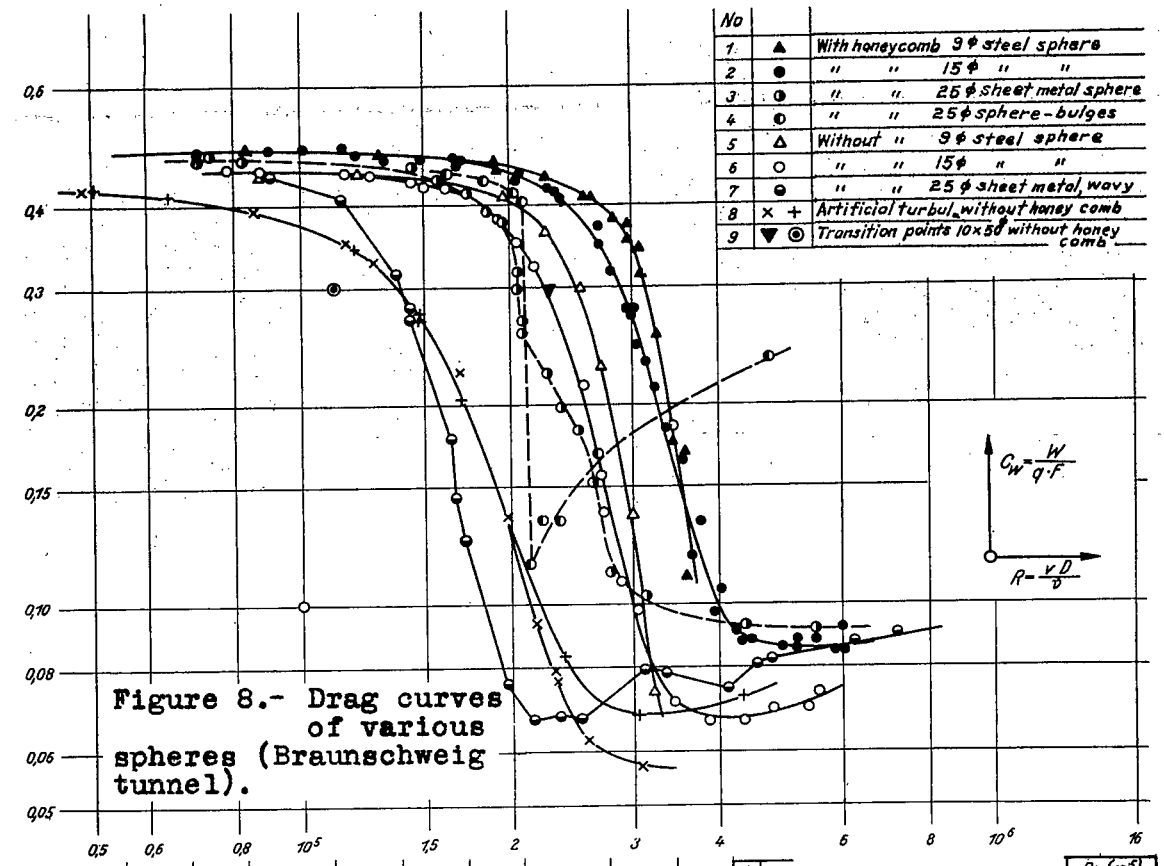

Figure 8.- Drag curves of various spheres (Braunschweig tunnel).

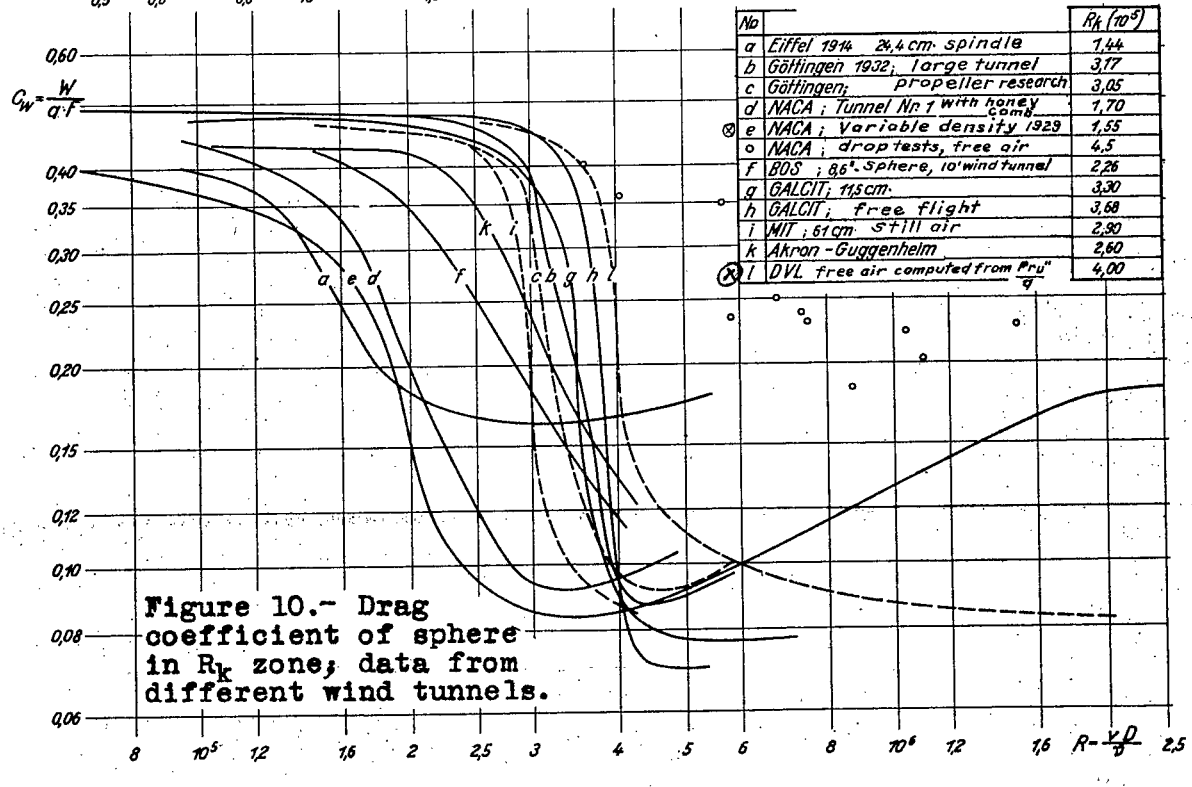

Figure 10.- Drag coefficient of sphere in R_k zone; data from different wind tunnels.

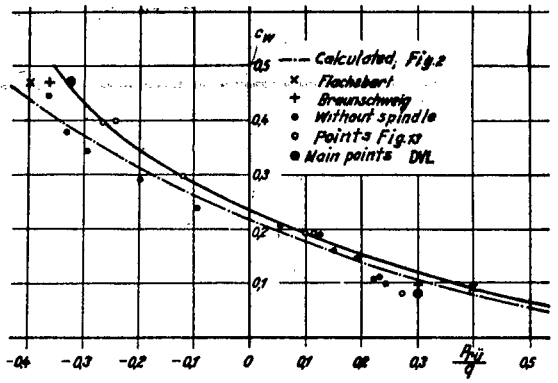

Figure 14.- Sphere drag in relation to pressure at back of sphere.

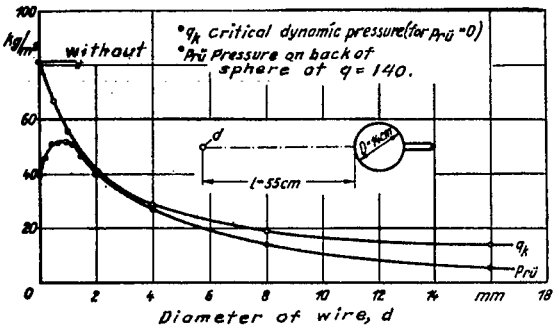

Figure 15.- Effect of different gage turbulence wires on critical dynamic pressure and super-critical sphere flow.

Figure 17.- Effect of lateral position of turbulence wires.

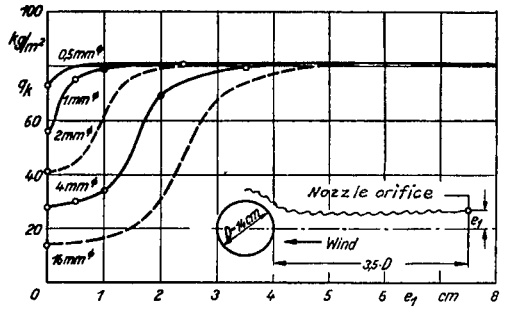

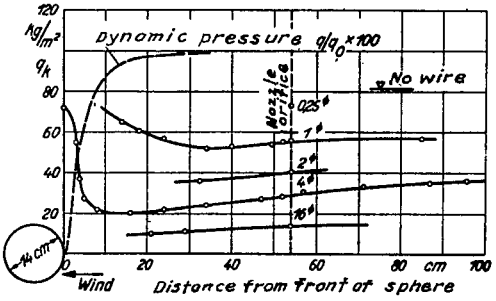

Figure 16.- Turbulence of wires fitted at varying distance up stream from sphere.

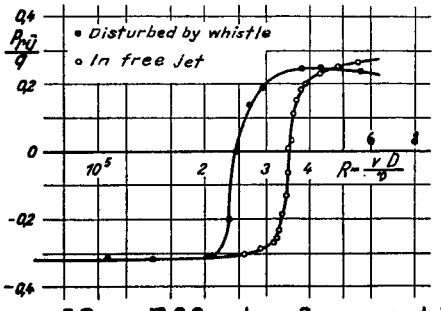

Figure 19.- Effect of acoustic air oscillations on the boundary layer of the sphere.

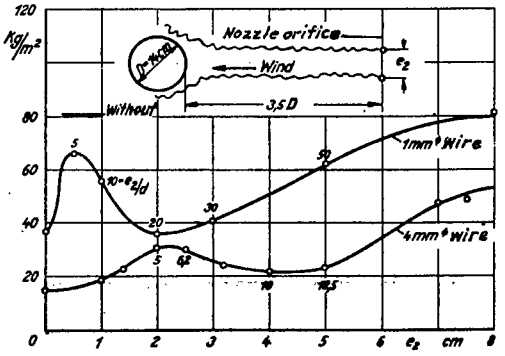

Figure 18.- Turbulence effect of pair of wires.

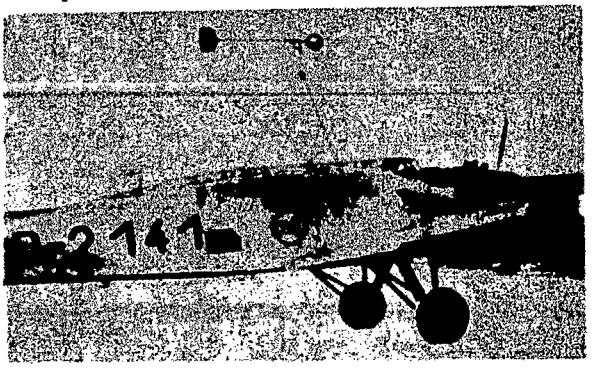

Figure 20. Method of mounting the 28 cm sphere on the Junkers W 34.

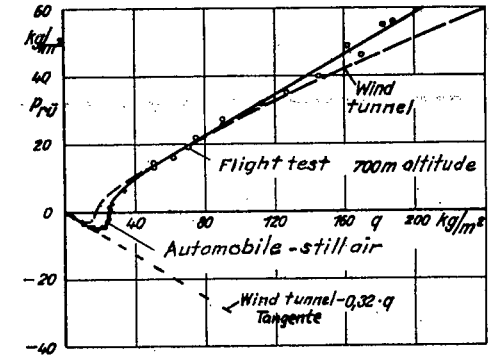

Figure 21.- Pressure curve of 28 cm sphere in still free air, touring-car and flight tests.

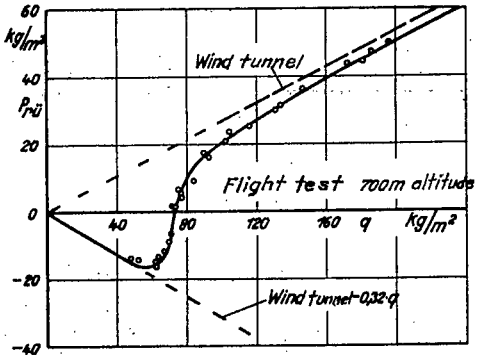

Figure 22.- Pressure curve of 15 cm steel sphere in flight.

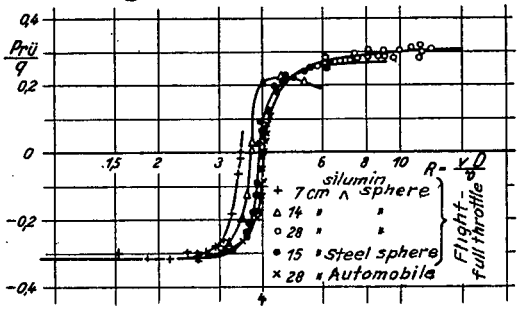

Figure 23.- Pressure curves of various spheres in air free from turbulence.

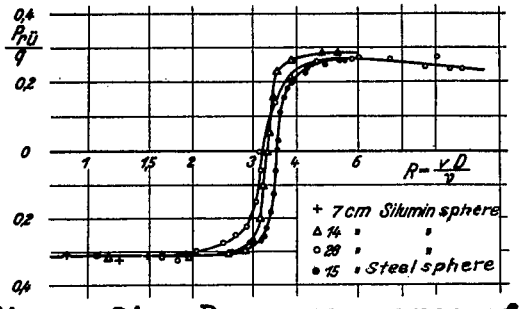

Figure 24.- Pressure curves of spheres in 1.2 m DVL tunnel.

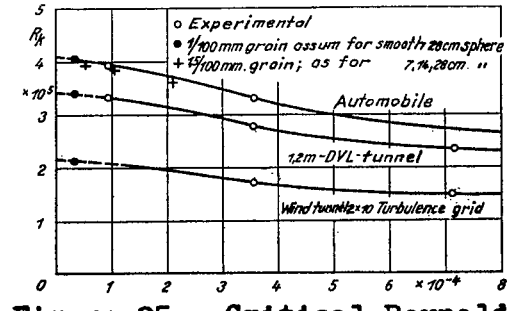

Figure 25.- Critical Reynolds Number of sphere versus surface roughness.

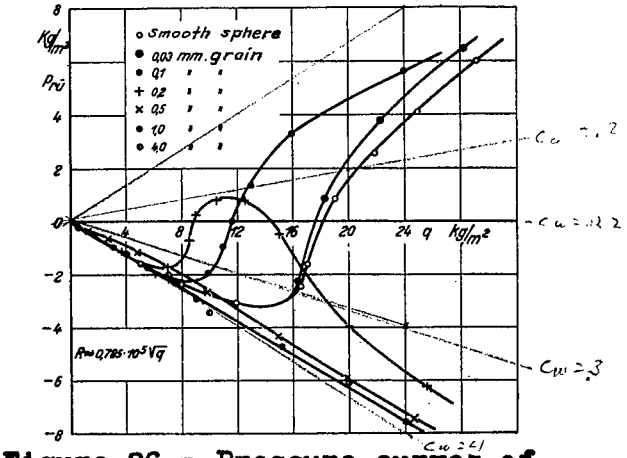

Figure 26.- Pressure curves of 28 cm sphere with varying degrees of roughness; 1.2 m DVL tunnel.

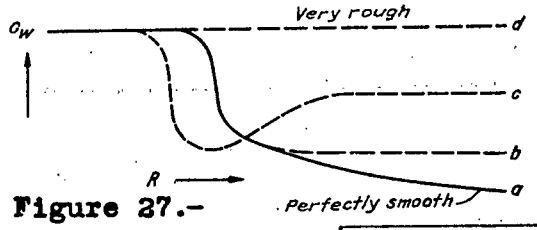

Figure 27.- Surface roughness versus sphere drag (schematically).

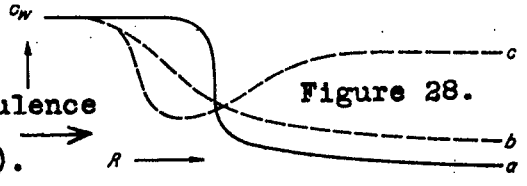

Figure 28. Effect of turbulence on sphere drag (schematically).